HHS Public Access

Author manuscript

J Phys Chem C Nanomater Interfaces. Author manuscript; available in PMC 2019 November 01.

Published in final edited form as:

J Phys Chem C Nanomater Interfaces. 2018 November 1; 122(43): 24740–24749. doi:10.1021/acs.jpcc.8b07365.

Effects of Deuteration of ^{13}C-Enriched Phospholactate on Efficiency of Parahydrogen-Induced Polarization by Magnetic Field Cycling

Oleg G. Salnikov[#a,b], **Roman V. Shchepin**[#c,d], **Nikita V. Chukanov**[#a,b], **Lamya Jaigirdar**[c,e], **Wellington Pham**[c,d,f,g], **Kirill V. Kovtunov**[a,b], **Igor V. Koptyug**[a,b], **Eduard Y. Chekmenev**[c,d,f,g,h,i,*]

[a]International Tomography Center, 3A Institutskaya St., Novosibirsk 630090, Russia

[b]Novosibirsk State University, 2 Pirogova St., Novosibirsk, 630090, Russia

[c]Vanderbilt University Institute of Imaging Science (VUIIS)

[d]Department of Radiology

[e]School of Engineering

[f]Department of Biomedical Engineering

[g]Vanderbilt-Ingram Cancer Center (VICC), Vanderbilt University, Nashville, Tennessee 37232-2310, United States

[h]Department of Chemistry, Integrative Biosciences (Ibio), Wayne State University, Karmanos Cancer Institute (KCI), Detroit, Michigan, 48202, United States

[i]Russian Academy of Sciences, Leninskiy Prospekt 14, Moscow, 119991, Russia

[#] These authors contributed equally to this work.

Abstract

We report herein a large-scale (>10 g) synthesis of isotopically enriched 1-^{13}C-phosphoenolpyruvate and 1-^{13}C-phosphoenolpyruvate-d_2 for application in hyperpolarized imaging technology. The 1-^{13}C-phosphoenolpyruvate-d_2 was synthesized with 57% overall yield (over two steps), and >98% ^{2}H isotopic purity, representing an improvement over the previous report. The same outcome was achieved for 1-^{13}C-phosphoenolpyruvate. These two unsaturated compounds with C=C bonds were employed for parahydrogen-induced polarization via pairwise parahydrogen addition in aqueous medium. We find that deuteration of 1-^{13}C-phosphoenolpyruvate resulted in overall increase of ^{1}H T_1 of nascent hyperpolarized protons (4.30 ± 0.04 s versus 2.06 ± 0.01 s) and ^{1}H polarization (~2.5% versus ~0.7%) of the resulting hyperpolarized 1-^{13}C-phospholactate. The nuclear spin polarization of nascent parahydrogen-derived protons was transferred to 1-^{13}C nucleus via magnetic field cycling procedure. The proton T_1 increase in hyperpolarized deuterated 1-^{13}C-phospholactate yielded approximately 30% better ^{13}C polarization compared to non-deuterated hyperpolarized 1-^{13}C-phospholactate. Analysis of T_1 relaxation revealed that deuteration of 1-^{13}C-phospholactate may have resulted in approximately

[*]**Corresponding Author**: chekmenev@wayne.edu.

3-fold worse H→^{13}C polarization transfer efficiency via magnetic field cycling. Since magnetic field cycling is a key polarization transfer step in the Side-Arm Hydrogenation approach, the presented findings may guide more rationale design of contrast agents using parahydrogen polarization of a broad range of ^{13}C hyperpolarized contrast agents for molecular imaging employing ^{13}C MRI. The hyperpolarized 1-^{13}C-phospholactate-d_2 is of biomedical imaging relevance because it undergoes in vivo dephosphorylation and becomes ^{13}C hyperpolarized lactate, which as we show can be detected in the brain using ^{13}C hyperpolarized MRI; an implication for future imaging of neurodegenerative diseases and dementia.

Graphical Abstract

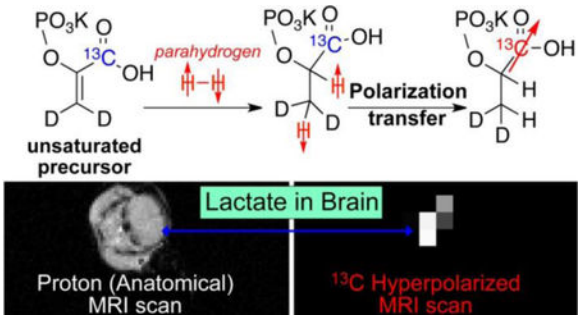

INTRODUCTION

Parahydrogen Induced Polarization (PHIP)[1–2] is a fast and efficient hyperpolarization technique.[3–8] When parahydrogen pairwise addition is performed to C=C or C≡C unsaturated chemical bond, the symmetry of nascent parahydrogen-derived protons can be broken due to their magnetic inequivalence in the product of this chemical reaction.[9–10] High-levels of polarization can be retained by the nascent protons.[11–15]

Because proton sites typically retain hyperpolarized (HP) state for a short period of time due to relatively short exponential decay time constants (e.g. spin-lattice relaxation time constant T_1) on the order of a few seconds,[16] the PHIP studies demonstrated a significant advantage of transferring parahydrogen-derived polarization to ^{13}C[13–15, 17] and ^{15}N sites with longer T_1 values on the order of a minute or more (Scheme 1a).[18] The resulting ^{13}C hyperpolarized (HP) compounds have been successfully employed as HP ^{13}C contrast agents to probe metabolism and biochemical functions in vivo as long as sufficiently high concentration and high polarization level can be achieved.[15, 19–29]

Two key approaches have been developed for polarization transfer from nascent parahydrogen-derived protons. In the first approach, radio-frequency (RF) pulses are employed, taking advantage of direct spin-spin couplings between the two protons and the ^{13}C nucleus.[14, 30–39] In the second approach, a magnetic field cycling (MFC) procedure is performed in weak magnetic fields (from nano-Tesla to tens of micro-Tesla) for spontaneous polarization transfer via the network of spin-spin couplings between parahydrogen-derived protons and the ^{13}C nucleus.[14–15, 20, 30, 40–41] The key advantage of the second approach is the possibility of longer-range polarization transfer over up to 5 chemical bonds away.[42] The

other advantage of MFC is a significantly less demanding hardware operations compared to RF-based methods: MFC requires a magnetic shield,[20, 40] whereas RF-based methods require a reasonably homogeneous magnet, RF coils, transmitters and other related hardware.[19, 24, 28, 34, 43–44] As a result, Side Arm Hydrogenation (SAH) approach has been developed,[42, 45–48] where parahydrogen (p-H_2) pairwise addition is performed into an ester moiety, and polarization is transferred to ^{13}C-carboxyl site, which has long T_1. Recently, PHIP-SAH has been demonstrated for efficient hyperpolarization of ^{13}C-acetate and ^{13}C-pyruvate moieties.[49–50] HP ^{13}C-acetate and ^{13}C-pyruvate have been shown to report on metabolic activities in cancers, liver disease, and brain.[51–64] Furthermore, PHIP-SAH HP 1-^{13}C-pyruvate has been shown recently to probe altered heart metabolism in vivo.[65]

Despite the recent progress with PHIP-SAH relying on MFC, ^{13}C hyperpolarization levels demonstrated to date are lower than those reported by dissolution Dynamic Nuclear Polarization (d-DNP; ^{13}C polarization, P_{13C} up to 60%[66]) and by PHIP relying of RF pulses (P_{13C} up to 59%[14, 67]).

The motivation of this work is to study the effect of deuteration on ^{13}C hyperpolarization relying on MFC procedure with the goal of improving the ^{13}C hyperpolarization yields. Here, we employed HP 1-^{13}C-phospholactate (PLAC) to study the effect of deuteration on the hyperpolarization via MFC, because HP PLAC can be converted to HP ^{13}C-lactate in vivo in vasculature,[68] and its imaging feasibility has already been shown.[28] To achieve this goal, we have prepared deuterated and non-deuterated forms of 1-^{13}C-phosphoenolpyruvate via improved synthetic procedure.[69] This unsaturated precursor is required for p-H_2 pairwise addition, which leads to formation of HP 1-^{13}C-phospholactate (Scheme 1b).

METHODS

General Considerations.

All glassware (round bottom flasks, magnetic stir bar, addition funnel, glass funnel and measuring cylinder) were oven dried.

Potassium 1-^{13}C-phosphoenolpyruvate-d_2 (PEP-d_2) synthesis.

1-^{13}C-pyruvic-d_4 acid (**1**) (10 g, 110 mmol, 1 eq) was added to a tared, oven-dried round bottom flask (previously flushed with Argon), immediately followed by the addition of carbon tetrachloride (40 mL). Then, the flask was equipped with an addition funnel for dispensing the mixture of bromine (~5.7 mL, 111 mmol, 1 eq) and carbon tetrachloride (~4 mL) into a stirring solution dropwise under the presence of argon over the course of 3 h at 4 °C (Figure S9). Upon bromine color disappearance (after 3 hours), the resulting mixture was evaporated in vacuo (0–2 mbar) with the co-solvent of methylene chloride (40 mL) and the process was repeated 3 times (3×40 mL of CH_2Cl_2 in total) until the solid material was dried completely to provide crude product **2** (16.7 g, 0.1 mol, 90% yield). The prepared crude material was used in the next step without purification, Scheme 2.

A solution of above-mentioned crude bromopyruvic acid (16.7 g, 0.1 mol) in anhydrous THF (50 mL) was added dropwise to a dried and argon-flushed round bottom flask (250-mL size) containing trimethyl phosphite, $P(OMe)_3$, (~1.1 eq., 14.8 mL, 125 mmol) and

anhydrous THF (50 mL) via an additional funnel at a rate that the reaction solution temperature never exceeded 45 °C. The round-bottom flask was equipped with magnetic stirrer, thermometer and addition funnel attached via a Claisen adapter (see Figure S10 for details). The mixture was stirred for 1h before the solvents were evaporated under the reduced pressure for 3 h. D_2O (80 mL) was added to the viscous residue until it was dissolved, and it was left stirring at RT overnight. Next, the mixture was transferred to an ice-chilled beaker and the pH was adjusted to approximately 2.8 using deuterated KOH (10 g KOH, 20 mL D_2O). Then, activated charcoal (0.5 g) was added to the solution, filtered, and the filtrate was evaporated under reduced pressure to provide solid **3**, which was re-dissolved in D_2O (100 mL) in the presence of activated charcoal (~0.5 g), filtered and the filtrate was evaporated under reduced pressure. The resulting solid was purified by recrystallization using water (~40 mL) and ethanol (~300 mL) to afford white crystal needles (13.1 g, 0.06 mol, 57% yield over two steps).

The produced material (1-^{13}C-phosphoenolpyruvate-d_2, **3**) was characterized by high-resolution NMR spectroscopy (Figures S5–S7) and by high-resolution mass spectrometry (HR-MS) (Figure S4).

^{13}C NMR (100 MHz, D_2O): 166.4. ^{31}P NMR (162 MHz, D_2O): −5.5. Proton characterization is not useful because of the deuteration.

HR-MS was performed by direct liquid infusion using an Orbitrap mass spectrometer (Thermo-Finnigan, San Jose, CA) equipped an Ion-Max source housing and a standard electrospray (ESI) ionization probe in negative ion mode at a resolving power of 60,000 (at m/z 400). $^{12}C_2{}^{13}C_1H_2D_2O_6P^-$ (M-H-): 169.99101; found 169.99079 (−1.3 ppm). The product ^{13}C isotopic purity was >99% (determined by the isotopic purity of the starting material), ^{2}H isotopic purity was >98% (determined from HR-MS and by NMR data).

Potassium 1-^{13}C-phosphoenolpyruvate (PEP) synthesis followed the same procedure as that for 1-^{13}C-phosphoenolpyruvate-d_2 described above with the exception that (i) D_2O was not employed (H_2O was used instead), and (ii) the starting material was 1-^{13}C-pyruvic acid (Isotec-Sigma-Aldrich, 677175). The overall synthesis is summarized in Scheme 3. The overall yield was similar to that for 1-^{13}C-phosphoenolpyruvate-d_2 reported above. The product ^{13}C isotopic purity was 99% in accord with the starting material enrichment employed in this synthesis: 1-^{13}C-pyruvic acid (Isotec-Sigma-Alrich, 677175). NMR spectroscopic characterization of the obtained product is provided in Figures S1–S3.

^{1}H NMR (400 MHz, D_2O): 5.43 (d.t., 1H, J = 10 Hz and 2.2 Hz), 5.77 (d.t., 1H, J = 3.5 Hz and 2.2 Hz). ^{13}C NMR (100 MHz, D_2O): 166.4 (d, J = 7 Hz). ^{31}P NMR (162 MHz, D_2O): −5.5.

NMR hyperpolarization.

Commercially available bis(norbornadiene)rhodium(I) tetrafluoroborate ($[Rh(NBD)_2]BF_4$, NBD = norbornadiene, Strem 45–0230), 1,4-bis[(phenyl-3-propanesulfonate)phosphine]butane (Sigma-Aldrich 717347) and ultra-pure hydrogen (H_2) (>99.999%) were used as received. The overall scheme of experimental setup is presented in

Figure 1. Hydrogen gas was enriched with p-H_2 up to 66–85% *para*-state using a home-made parahydrogen generator. p-H_2 gas flow rate was regulated with mass flow controller (SmartTrak 50, Sierra Instruments, Monterey, CA). The previously described procedure[32] was used for the preparation of homogeneous catalyst solution in D_2O (~5.3 mM) followed by addition of PEP or PEP-d_2 to obtain approximately 30 mM substrate concentration. Medium-wall 5 mm NMR tubes (Wilmad glass P/N 503-PS-9) tightly connected with ¼ in. outer diameter PTFE tubes were filled with 0.5 mL of resultant solution under argon atmosphere and pressurized with p-H_2 up to 70 psig. The samples were preheated either up to 60 °C using NMR spectrometer temperature control unit (in case of PASADENA[9–10] experiments) or up to ~70–80 °C using hot water (in case of ALTADENA[70] and MFC experiments). The p-H_2 gas was bubbled at 140 standard cubic centimeters per minute (sccm) flow rate and 70 psig pressure. In PASADENA experiments, the sample was located inside the probe of 9.4 T Bruker NMR spectrometer during p-H_2 gas bubbling, while in ALTADENA and MFC experiments p-H_2 gas was bubbled while the sample was located in the Earth's magnetic field. After termination of p-H_2 bubbling the sample was either transferred directly to the NMR probe (in ALTADENA experiments) or placed inside the mu-metal magnetic shield described in detail in Ref. # [41] in experiments employing MFC polarization transfer. The magnetic field inside the shield was adjusted using additional solenoids placed inside the mu-metal shield (Note the mu-metal shield provides an isolation of approximately 1,200 according to the manufacturer's specification; therefore, the use of the shield in the Earth's magnetic field results in the minimum residual magnetic field of approximately 40 nT). Then the sample was slowly (~1 s) pulled out of the shield and placed inside the NMR probe for detection. PHIP spectra were acquired as pseudo 2D sets consisting of 64 ^{1}H NMR spectra in order to avoid delays between placing the sample into the probe and starting of the acquisition. The acquisition of these pseudo 2D sets was always started before termination of p-H_2 bubbling, and the first spectra containing signal were used for presentation here. In PASADENA experiments NMR spectra were acquired using 45° RF excitation pulse, while in ALTADENA and MFC experiments 90° RF pulse was used. Note that in all experiments the temperature of the sample inside the NMR probe was set to 60° C using NMR spectrometer temperature control unit. The sample transfer time in and out of the shield was approximately 2 seconds, and the sample transfer time into 9.4 T NMR spectrometer was ~5–6 seconds.

PLAC-d_2 hyperpolarization for *in vivo* experiments was performed as described previously.[28, 69] The resulting mixture contained approximately 25 mM of HP PLAC-d_2 with $\%P_{13C}$ ~ 5%.

Calculation of NMR Signal Enhancement and Nuclear Spin Polarization.

^{1}H and ^{13}C NMR signal enhancement factors (ε_{1H} and ε_{13C}, respectively) were calculated using NMR signals of thermally polarized 1-^{13}C-phospholactate molecules as a reference, according to formulas:

$$\varepsilon_{1H} = \frac{I_{1H-HP}}{I_{1H-PLac}} \times N_{1H-PLac}$$

$$\varepsilon_{13C} = \frac{I_{13C-HP}}{I_{13C-PLac}}$$

where $I_{1H\text{-}HP}$, $I_{1H\text{-}PLac}$, $I_{13C\text{-}HP}$ and $I_{13C\text{-}PLac}$ are, respectively, ^{1}H and ^{13}C NMR signal intensities of HP and thermally polarized PLAC after hydrogenation reaction ($I_{1H\text{-}HP}$ and $I_{1H\text{-}PLac}$ are signals of methyl group), $N_{1H\text{-}PLac}$ is the number of protons in the methyl group of corresponding PLAC molecule ($N_{1H\text{-}PLac}$ = 3 for non-deuterated PLAC and $N_{1H\text{-}PLac}$ = 1 for PLAC-d_2).

Nuclear spin polarizations P_{1H} and P_{13C} were calculated using the formula

$$P = \varepsilon \times P_0$$

where P_0 is the equilibrium nuclear spin polarization of ^{1}H or ^{13}C at the 9.4 T magnetic field and 333 K temperature ($P_0 = 2.9\times10^{-3}$% for ^{1}H and $P_0 = 7.2\times10^{-4}$% for ^{13}C). Because experiments were performed with broadly varied p-H_2 fraction (66–85%), the observed polarizations were also recalculated to the highest utilized p-H_2 fraction (85%) for the sake of comparison using the formula[4]

$$P_{85\%} = P \times \frac{4 \times 0.85 - 1}{4\chi_p - 1}$$

where $P_{85\%}$ is polarization recalculated to 85% p-H_2 fraction and χ_p is the p-H_2 fraction employed in particular experiment.

RESULTS AND DISCUSSION

Synthesis of potassium 1-^{13}C-phosphoenolpyruvate-d_2 (PEP-d_2).

The overall yield (over two steps) was 57%, which represents an improvement over the previously reported 43% yield.[69] The isotopic ^{13}C enrichment was ~99%. The deuterium isotopic purity was >98%, which is significantly better than the previously reported procedure, which reported ~80% deuterium isotopic purity.[69] The synthesis was repeated several times (N>3), and the yields and material purity were reproducible for both PEP-d_2 and PEP. All reported improvements can be primarily attributed to a better source of the starting material: 1-^{13}C-pyruvic-d_4 acid (Isotec-Sigma-Aldrich) versus previously employed 1-^{13}C-pyruvic acid (Isotec-Sigma-Aldrich 677175), which was deuterated in the first step. We note that the overall yield is consistent with the previous reports for preparation of unlabeled phosphoenolpyruvate,[71] although the prior reports with the exception of Ref. # [69] did not perform deuteration of phosphoenolpyruvate. The overall purity (~99%) of the synthesized PEP-d_2 was assessed by ^{31}P NMR spectroscopy (Figure S6). It compares favorably to our previous report for PEP-d_2 of overall purity of ~96.3% (Figure S5 from Ref. # [69]).

^{1}H PHIP Hyperpolarization.

^{1}H hyperpolarization of 1-^{13}C-phospholactate and 1-^{13}C-phospholactate-d_2 via PASADENA and ALTADENA protocols was investigated (see Figure 2a and Figure 3a). It was found that PASADENA protocol (hydrogenation in the high magnetic field) was significantly more efficient than ALTADENA protocol (hydrogenation in the Earth's magnetic field with subsequent transfer of the sample to the high field for detection). For example, for non-deuterated 1-^{13}C-phospholactate ε_{1H} was ~240 in PASADENA experiment presented in Figure 2b–c, whereas in ALTADENA experiments presented in Figure 3b–c ε_{1H} was only ~17. Similar results were obtained for 1-^{13}C-phospholactate-d_2: ε_{1H} in PASADENA experiment presented in Figure 2d–e was ~3 times greater than in ALTADENA experiments presented in Figure 3d–e (~640 vs. ~220). Importantly, it was found that deuteration of the PEP allows obtaining significantly higher ^{1}H polarization of the resultant phospholactate (P_{1H} ~2.5% for phospholactate-d_2 vs. P_{1H} ~0.71% for non-deuterated phospholactate at 85% p-H_2 fraction and in the case of PASADENA experimental protocol, see Table S1).

Polarization transfer to ^{13}C nucleus via Magnetic Field Cycling (MFC).

MFC experiments were performed for the transfer of polarization to ^{13}C nuclei of 1-^{13}C-phospholactate molecules. First, magnetic field profile of ^{13}C polarization was obtained at the optimal in terms of resulting ^{1}H polarization duration of p-H_2 bubbling (Figure 4). It was found that the optimal magnetic field for MFC experiments is ~0.05 μT. The maximum ^{13}C polarization for PLAC-d_2 was ~1.3 times higher than that for non-deuterated PLAC (P_{13C} ~0.10% (ε_{13C} ~ 104) or for phospholactate-d_2 vs. P_{13C} ~0.078% (ε_{13C} ~ 85) for non-deuterated 1-^{13}C-phospholactate at 85% p-H_2 fraction, see Figure 5a (the schematic of the process), Figure 5b (the ^{13}C spectrum of HP 1-^{13}C-phospholactate), Figure 5c (the ^{13}C spectrum of thermally polarized 1-^{13}C-phospholactate after HP state decay seen in Figure 5b), Figure 5d (the ^{13}C spectrum of HP 1-^{13}C-phospholactate-d_2), Figure 5e (the ^{13}C spectrum of thermally polarized 1-^{13}C-phospholactate-d_2 after HP state decay seen in Figure 5d) and Table S2).

Spin-lattice T_1 relaxation results of hyperpolarized ^{1}H and ^{13}C sites and its influence on the levels of obtained polarization.

The first advantage of the use of deuterated precursors for production of HP biomolecules is the reduction of the number of proton spins, which reduces the complexity of the spin system,[69, 73] and it was found helpful for improving polarization transfer efficiency by methods relying on RF-based polarization transfer. [22–23, 69] The second advantage of deuteration is the usually observed increase of hyperpolarization lifetime.[22–23, 69, 74–75] Indeed, ^{1}H T_1 measurements at 9.4 T magnetic field yielded T_1 = 2.06 ± 0.01 s for non-deuterated PLAC and T_1 = 4.30 ± 0.04 s for PLAC-d_2, that is ~2 times difference. In contrast, ^{13}C T_1 measurements at the same field resulted in T_1 = 16.26 ± 0.04 s for non-deuterated PLAC and 12.98 ± 0.09 s for PLAC-d_2. We expect ^{1}H and ^{13}C T_1 values to be similar at high (9.4 T) and low (the Earth's and micro-Tesla) magnetic fields based on recently published relaxation study of metronidazole.[72]

First, and foremost, because ^{1}H T_1 values are significantly lower than the sample transfer time (ca. 5–6 s), significant polarization losses occur during the sample transfer. Not

surprisingly, PASADENA signal enhancements (when the sample was reacted inside the NMR spectrometer, and the sample transfer was not needed) were significantly greater than those obtained using ALTEDENA approach. The effect is more pronounced for non-deuterated HP PLAC, because it has more than 2-fold lower T_1 of HP protons than that in PLAC-d_2. Therefore, the fact that the resulting PASADENA ^1H signal enhancement for PLAC (ε_{1H} ~240) was significantly lower than that for PLAC-d_2 (ε_{1H} ~640) can be explained by greater depolarization of nascent HP protons during 5-second-long p-H_2 bubbling. Moreover, the additional time interval of ~5–6 seconds required for sample transfer caused disproportionately greater polarization losses in ALTADENA hyperpolarization of PLAC (ε_{1H} ~17) versus PLAC-d_2 (ε_{1H} ~220). Thus, generally the higher ^1H signal enhancements observed for PLAC-d_2 versus those detected in PLAC can be explained by longer lifetime of ^1H polarization.

It should be noted that in MFC experiments the lifetime of ^1H polarization is important, because hyperpolarization is initially generated on protons while the unsaturated precursor is hydrogenated in the Earth's magnetic field. Thus, the relaxation of hyperpolarization before the step of polarization transfer to ^{13}C nuclei may have significant implications on the resulting ^{13}C polarization. To this extent, the maximum obtained ^{13}C signal enhancement levels in PLAC (ε_{13C} ~ 85) and PLAC-d_2 (ε_{13C} ~ 104) are unexpected, because since PLAC-d_2 has significantly longer ^1H T_1 values, one would expect ε_{13C} to be several-fold greater in PLAC-d_2 vs. PLAC. Because ^{13}C T_1 values are significantly greater than the sample transfer time (and quite similar for both PLAC and PLAC-d_2), the ^{13}C polarization losses due to T_1 relaxation after polarization transfer are likely relatively small for both substrates (< 40%). When the observed PASADENA ^1H polarization levels are employed for computing the efficiency of polarization transfer from nascent protons to ^{13}C, the resulting efficiencies are relatively low: 0.078%/0.71% or ~11% for PLAC and 0.1%/2.5% or ~4% for PLAC-d_2. While arguably some ^1H polarization losses have occurred during ~2-second-long sample manipulation delay (between cessation of p-H_2 bubbling and sample insertion in the magnetic shield), and they have caused the apparent reduction of polarization transfer efficiency, PLAC was likely penalized disproportionately more by these relaxation losses, because PLAC ^1H T_1 is more than a factor of two lower than that of PLAC-d_2 (and therefore reducing the apparent value of the polarization transfer efficiency more in PLAC vs. PLAC-d_2). To summarize, the polarization transfer efficiency from nascent p-H_2 protons to ^{13}C nucleus by the magnetic field cycling process appears to be nearly threefold worse in the deuterated PLAC-d_2 compared to non-deuterated PLAC. We note that if the analysis of polarization losses due to T_1 relaxation is not taken into account, one may arrive to a conclusion that deuteration is helpful for the MFC efficiency, because the maximum obtained ^{13}C signal enhancements were better (by a factor of ~1.3) for PLAC-d_2 versus PLAC. The latter observation is likely caused by longer proton T_1 values for PLAC-d_2 versus those for PLAC. A potential explanation of the worse polarization transfer efficiency in deuterated PLAC-d_2 is polarization transfer from p-H_2-derived protons to deuterons.[76] However, we note that the experimental results presented here had the following limitations. First and foremost, the reproducibility of the data was significantly impacted by a very short T_1 values of proton sites and relatively short T_1 values of ^{13}C sites. As a result, a small variation (e.g. ~0.5–1 second for PLAC with proton T_1 of ~2 s) in the duration of the sample

manipulation (especially during field cycling and hydrogenation, when the decay of polarization is governed by proton T_1 values) would have a substantial overall effect on the observed signal and polarization values, and would have significantly impacted shot-to-shot reproducibility of our data. Second, the duration of the field cycling was manually controlled, and it is estimated to be in the range between 0.5 and 1.5 seconds. This variability would also inevitably have impacted the data reproducibility for the magnetic field plots shown in Figure 4. Third, the exact values for T_1 in the low and nano-Tesla magnetic field regimes have not been determined here, but may have a significant effect on the overall polarization transfer. The last but not the least, it is very surprising that it is the deuterated sample that shows more significant polarization fluctuations with small changes in the low-field value—note that over the entire range of fields explored, the ^{2}H Zeeman precession rate is << 1 Hz, so for a low-field residence time of < 1s, the ^{2}H precession angle is quite small. It is therefore somewhat puzzling how the exact value of the field could affect the outcome so much. The latter question can clearly benefit from in-depth theoretical investigations and simulations, which are certainly warranted. Furthermore, it is entirely possible that the optimization of the field cycling procedure (i.e. the timing and the amplitude of the field sweep), may significantly impact the polarization transfer efficiency in deuterated versus non-deuterated compounds. Despite the above-mentioned limitations, to the best of our knowledge, this work is the first report highlighting that deuteration of the substrate maybe detrimental to polarization transfer from parahydrogen-derived protons to ^{13}C nucleus in the context of magnetic field cycling methods for polarization transfer.

Outlook for contrast agent development by MFC.

The efficient relaxation processes can be a significant practical limitation for the use of HP contrast agents. In the current study, the ^{1}H polarization losses due to efficient relaxation during ~5 s long reaction time have caused significant reduction of polarization of nascent protons. Moreover, only a small fraction of material was converted during ~5-second-long reaction time (less than 20%, Figure S8). Both of these issues can be potentially remedied through use of high-pressure PHIP hyperpolarizers, where PHIP precursors can be reacted on the time scale significantly shorter than ^{1}H T_1.[19, 24, 28–29, 34, 77–78] From the practical perspective, the use of PHIP moieties with long T_1 values will be beneficial to maximize the level of polarization through minimization of relaxation losses. Such moieties may include allyl side arm,[49–50] and others.[41] While PHIP precursor deuteration is helpful in the context of RF-based methods,[13–14, 23, 67, 69] the data presented here points that deuteration (while helpful to increase proton T_1 values) may be detrimental to the efficiency of polarization transfer via magnetic field cycling approach.[20]

Feasibility of brain imaging with HP PLAC-d_2.

5XFAD mice were maintained at Vanderbilt University under standard conditions, in a 12-h light/dark cycle and with free access to food and water, as we described in the past.[79] The 5XFAD mice over express both mutant human APP and PS1, correlating with high burden and accelerated accumulation of the Aβ. A colony of 5XFAD transgenic mice obtained from Jackson Laboratories was maintained by crossing 5XFAD mice with a wild-type (wt) C57BL/6J strain. The mice were genotyped by a standard polymerase chain reaction using DNA isolated from tail tips with the following primers: PSEN1 forward, 5'–

TCATGACTATCCTCCTGGTGG-3' and reverse, 5'-CGTTATAGGTTTTAAACACTTCCCC-3'. For APP, forward, 5' -AGGACTGACCACTCGACCAG-3' and reverse, 5'-CGGGGGTCTAGTTCTGCAT-3'. We also genotyped mice for the presence of retinal degeneration Pde6brd1 mutation using forward, 5'-AAGCTAGCTGCAGTAACGCCATTT-3' and reverse, 5'-ACCTGCATGTGAACCCAGTATTCTATC-3'. After polymerase chain reaction amplification, the DNA product of each reaction was analyzed by size fractionation through a 1% agarose gel; with Pde6b mutant = 560bp, APP transgene = 377bp and PSEN1 transgene = 608bp. The 5XFAD mice were maintained as heterozygous. Animal experiments were conducted per the guidelines established by Vanderbilt University's Institutional Animal Care and Use Committee. At the end of the study, animals were euthanized by cervical dislocation after sedation with isoflurane. Clinical signs were used to verify euthanasia, including heartbeats and reflection to toe-pinching. Further, if animals showed signs of illness (weight loss, food withdrawal, or infection) they were sacrificed before the endpoints. All experimental procedures in this study were approved by the Vanderbilt University IACUC panel.

Mouse tail-vein catheter.

An in-house generated catheter was comprised of detached insulin needle cannula (30G) inserted into a catheter (Micro-Renathane Implantation Tubing), of which, the other end was inserted with a needle (28G) hub for filling heparin (1%)-based saline to prevent blood clotting. Intravenous (IV) insertion of the catheter on a ketamine/xylazine (0.15 mg/g/0.01 mg/g)-induced mouse was started with the insertion of the needle at either side of the lateral veins. Appropriate IV catheter preparation was evidenced and confirmed only when copious amount of blood appeared in the catheter (Figure 6a). Then, the animal was aligned on the MRI holder equipped with designated surface RF coils before MRI (Figure 6b). The holder containing the animal and ^{13}C surface RF coils was placed inside a volume ^{1}H RF coil. HP molecular probe injection was performed via the catheter while the animal was appropriately aligned inside the magnet with heartbeat and body temperature monitoring.

Animal imaging study.

Because the overall ^{13}C polarization levels achieved using MFC were relatively low, the *in vivo* experiments proceeded with high-pressure hyperpolarizer with polarization transfer implemented with the use of RF pulses. The RF pulse sequence developed by Goldman and co-workers[13] was employed as described previously.[28]

The level of hyperpolarization of HP PLAC-d_2 was checked *in situ* of the hyperpolarizer as described previously.[28, 69] The HP PLAC-d_2 solution was ejected in a plastic syringe and buffered for a pH with a solution of phosphate buffer. Approximately 0.2 mL of resulting HP liquid was injected via tail vein, and non-localized MR spectroscopy was recorded using approximately 15° RF excitation pulse. The MRS recorded every ~3 seconds (Figure 6e) shows initial contrast agent delivery to the brain, which is observed as initial signal growth followed by the decay of HP signal. We note that the PLAC undergoes fast dephosphorylation *in vivo* and becomes HP 1-^{13}C-lactate as discussed previously,[29, 68] although ^{13}C chemical shift of HP PLAC-d_2 and HP ^{13}C-lactate-d_2 are indistinguishable,

because the chemical shift difference of ~0.3 ppm[68] could not be resolved *in vivo*. Only one ^{13}C HP NMR resonance was detected. The overall HP dynamics of PLAC-d_2 is similar to that reported for mice previously.[28]

2D HP ^{13}C imaging was performed using gradient-echo sequence (GRE, under GEMS name on Varian platform) without slice selection. The slice selection is effectively achieved through the use of the surface RF coil, which has a limited excitation range immediately under the RF coil (see Figure 6b). The 2D ^{13}C image with the highest intensity is shown in Figure 6d corresponding to the maximum determined by the MRS (in Figure 6e). Comparison with ^{1}H anatomical imaging recorded using the volume RF coil (Figure 6c) shows that the HP signal indeed originates from the brain rather than other parts of mouse head.

The pilot data presented in Figure 6 shows a promise of HP PLAC-d_2 for molecular imaging of brain metabolism in a manner similar to that using HP compounds produced by d-DNP.[57] The use of more advanced RF pulse sequence is certainly warranted to improve spectral, temporal and spatial resolution of HP images.[80–81]

CONCLUSION

To conclude, we have reported on large–scale (>10 g) synthesis of PEP-d_2 and PEP, which serves as precursors for parahydrogen induced polarization of PLAC-d_2 and PLAC, respectively with ~57% yield and >98% deuterium purity (for PEP-d_2), which represents an improvement over the previous report. The deuteration enhances T_1 of nascent HP protons by approximately 2-fold, which is a clear advantage, because it minimizes T_1-associated-polarization losses during hyperpolarization procedure. At the same time, the deuteration of PEP leads to approximately 3 times worse $^{1}H \rightarrow ^{13}C$ polarization transfer efficiency via magnetic field cycling, which is a disadvantage in the context of developing HP contrast agents for biomedical imaging applications, where high polarization level is required. These findings will be helpful for more rationale design of HP molecular precursors for development of HP contrast agents by PHIP especially in the context of SAH approach. The pilot use of HP PLAC-d_2 (produced using RF-based approach to enhance $\%P_{13C}$ to ~ 5%) is demonstrated for *in vivo* spectroscopy and imaging of brain metabolism in mouse model of Alzheimer's disease.

Supplementary Material

Refer to Web version on PubMed Central for supplementary material.

ACKNOWLEDGEMENTS

O.G.S., N.V.C. and K.V.K. thank the Russian Science Foundation (grant #17-73-20030) for the support with preparation of isotopically labeled compounds. This work was supported by NSF under grant CHE-1416432 (EC) and CHE-1836308 (EC), 1R21EB020323 (EC), 1R21CA220137 (EC), and R01 CA160700 (WP), DOD CDMRP BRP W81XWH-12-1-0159/BC112431 (EC) and RFBR 17-54-33037-OHKO_a (I.V.K.). Russian team thanks the Federal Agency for Scientific Organizations #0333-2017-0002 for the support to studies of H_2 activation. We thank Dr. Aaron M. Coffey for assistance with PHIP polarizer and preparation of HP PLAC-d_2 and image processing.

REFERENCES

1. Eisenschmid TC; Kirss RU; Deutsch PP; Hommeltoft SI; Eisenberg R; Bargon J; Lawler RG; Balch AL Para Hydrogen Induced Polarization in Hydrogenation Reactions. J. Am. Chem. Soc 1987, 109, 8089–8091.
2. Natterer J; Bargon J Parahydrogen Induced Polarization. Prog. Nucl. Mag. Res. Spectrosc 1997, 31, 293–315.
3. Barskiy DA; Coffey AM; Nikolaou P; Mikhaylov DM; Goodson BM; Branca RT; Lu GJ; Shapiro MG; Telkki V-V; Zhivonitko VV, et al. NMR Hyperpolarization Techniques of Gases. Chem. Eur. J 2017, 23, 725–751. [PubMed: 27711999]
4. Hövener J-B; Pravdivtsev AN; Kidd B; Bowers CR; Glöggler S; Kovtunov KV; Plaumann M; Katz-Brull R; Buckenmaier K; Jerschow A, et al. Parahydrogen-Based Hyperpolarization for Biomedicine. Angew. Chem. Int. Ed 2018, 57, 11140–11162.
5. Kovtunov KV; Pokochueva E; Salnikov OG; Cousin S; Kurzbach D; Vuichoud B; Jannin S; Chekmenev EY; Goodson BM; Barskiy DA, et al. Hyperpolarized NMR: D-DNP, PHIP, and SABRE. Chem. Asian J 2018, 13, 1857–1871.
6. Goodson BM; Whiting N; Coffey AM; Nikolaou P; Shi F; Gust BM; Gemeinhardt ME; Shchepin RV; Skinner JG; Birchall JR, et al. Hyperpolarization Methods for MRS. Emagres 2015, 4, 797–810.
7. Green RA; Adams RW; Duckett SB; Mewis RE; Williamson DC; Green GGR The Theory and Practice of Hyperpolarization in Magnetic Resonance Using Parahydrogen. Prog. Nucl. Mag. Res. Spectrosc 2012, 67, 1–48.
8. Kovtunov KV; Zhivonitko VV; Skovpin IV; Barskiy DA; Koptyug IV Parahydrogen-Induced Polarization in Heterogeneous Catalytic Processes. Top. Curr. Chem 2013, 338, 123–180. [PubMed: 23097028]
9. Bowers CR; Weitekamp DP Transformation of Symmetrization Order to Nuclear-Spin Magnetization by Chemical-Reaction and Nuclear-Magnetic-Resonance. Phys. Rev. Lett 1986, 57, 2645–2648. [PubMed: 10033824]
10. Bowers CR; Weitekamp DP Para-Hydrogen and Synthesis Allow Dramatically Enhanced Nuclear Alignment. J. Am. Chem. Soc 1987, 109, 5541–5542.
11. Zhao EW; Maligal-Ganesh R; Xiao C; Goh T-W; Qi Z; Pei Y; Hagelin-Weaver HE; Huang W; Bowers CR Silica-Encapsulated Pt-Sn Intermetallic Nanoparticles: A Robust Catalytic Platform for Parahydrogen-Induced Polarization of Gases and Liquids. Angew. Chem. Int. Ed 2017, 56, 3925–3929.
12. Salnikov OG; Barskiy DA; Coffey AM; Kovtunov KV; Koptyug IV; Chekmenev EY Efficient Batch-Mode Parahydrogen-Induced Polarization of Propane. ChemPhysChem 2016, 17, 3395–3398. [PubMed: 27459542]
13. Goldman M; Johannesson H Conversion of a Proton Pair Para Order into C-13 Polarization by RF Irradiation, for Use in MRI. C. R. Physique 2005, 6, 575–581.
14. Goldman M; Johannesson H; Axelsson O; Karlsson M Design and Implementation of C-13 Hyperpolarization from Para-Hydrogen, for New MRI Contrast Agents. C. R. Chimie 2006, 9, 357–363.
15. Golman K; Axelsson O; Johannesson H; Mansson S; Olofsson C; Petersson JS Parahydrogen-Induced Polarization in Imaging: Subsecond C-13 Angiography. Magn. Reson. Med 2001, 46, 1–5. [PubMed: 11443703]
16. Barskiy DA; Salnikov OG; Shchepin RV; Feldman MA; Coffey AM; Kovtunov KV; Koptyug IV; Chekmenev EY NMR SLIC Sensing of Hydrogenation Reactions Using Parahydrogen in Low Magnetic Fields. J. Phys. Chem. C 2016, 120, 29098–29106.
17. Bhattacharya P; Harris K; Lin AP; Mansson M; Norton VA; Perman WH; Weitekamp DP; Ross BD Ultra-Fast Three Dimensional Imaging of Hyperpolarized C-13 in Vivo. Magn. Reson. Mater. Phy 2005, 18, 245–256.
18. Bales L; Kovtunov KV; Barskiy DA; Shchepin RV; Coffey AM; Kovtunova LM; Bukhtiyarov AV; Feldman MA; Bukhtiyarov VI; Chekmenev EY, et al. Aqueous, Heterogeneous Parahydrogen-Induced 15N Polarization. J. Phys. Chem. C 2017, 121, 15304–15309.

19. Kadlecek S; Vahdat V; Nakayama T; Ng D; Emami K; Rizi R A Simple and Low-Cost Device for Generating Hyperpolarized Contrast Agents Using Parahydrogen. NMR Biomed 2011, 24, 933–942. [PubMed: 21845739]
20. Johannesson H; Axelsson O; Karlsson M Transfer of Para-Hydrogen Spin Order into Polarization by Diabatic Field Cycling. C. R. Physique 2004, 5, 315–324.
21. Olsson LE; Chai C-M; Axelsson O; Karlsson M; Golman K; Petersson JS MR Coronary Angiography in Pigs with Intraarterial Injections of a Hyperpolarized 13C Substance. Magn. Reson. Med 2006, 55, 731–737. [PubMed: 16538605]
22. Bhattacharya P; Chekmenev EY; Perman WH; Harris KC; Lin AP; Norton VA; Tan CT; Ross BD; Weitekamp DP Towards Hyperpolarized 13C-Succinate Imaging of Brain Cancer. J. Magn. Reson 2007, 186, 150–155. [PubMed: 17303454]
23. Chekmenev EY; Hovener J; Norton VA; Harris K; Batchelder LS; Bhattacharya P; Ross BD; Weitekamp DP Pasadena Hyperpolarization of Succinic Acid for MRI and NMR Spectroscopy. J. Am. Chem. Soc 2008, 130, 4212–4213. [PubMed: 18335934]
24. Hövener J-B; Chekmenev EY; Harris KC; Perman W; Robertson L; Ross BD; Bhattacharya P Pasadena Hyperpolarization of 13C Biomolecules: Equipment Design and Installation. Magn. Reson. Mater. Phy 2009, 22, 111–121.
25. Bhattacharya P; Chekmenev EY; Reynolds WF; Wagner S; Zacharias N; Chan HR; Bünger R; Ross BD Parahydrogen-Induced Polarization (PHIP) Hyperpolarized Mr Receptor Imaging in Vivo: A Pilot Study of 13C Imaging of Atheroma in Mice. NMR Biomed 2011, 24, 1023–1028. [PubMed: 21538638]
26. Zacharias NM; Chan HR; Sailasuta N; Ross BD; Bhattacharya P Real-Time Molecular Imaging of Tricarboxylic Acid Cycle Metabolism in Vivo by Hyperpolarized 1-C-13 Diethyl Succinate. J. Am. Chem. Soc 2012, 134, 934–943. [PubMed: 22146049]
27. Zacharias NM; McCullough CR; Wagner S; Sailasuta N; Chan HR; Lee Y; Hu J; Perman WH; Henneberg C; Ross BD, et al. Towards Real-Time Metabolic Profiling of Cancer with Hyperpolarized Succinate. J. Mol. Imaging Dyn 2016, 6, 123. [PubMed: 27547490]
28. Coffey AM; Shchepin RV; Truong ML; Wilkens K; Pham W; Chekmenev EY Open-Source Automated Parahydrogen Hyperpolarizer for Molecular Imaging Using 13C Metabolic Contrast Agents. Anal. Chem 2016, 88, 8279–8288. [PubMed: 27478927]
29. Coffey AM; Feldman MA; Shchepin RV; Barskiy DA; Truong ML; Pham W; Chekmenev EY High-Resolution Hyperpolarized in Vivo Metabolic 13C Spectroscopy at Low Magnetic Field (48.7 mT) Following Murine Tail-Vein Injection. J. Magn. Reson 2017, 281, 246–252. [PubMed: 28651245]
30. Goldman M; Johannesson H; Axelsson O; Karlsson M Hyperpolarization of C-13 through Order Transfer from Parahydrogen: A New Contrast Agent for MFI. Magn. Reson. Imaging 2005, 23, 153–157. [PubMed: 15833606]
31. Kadlecek S; Emami K; Ishii M; Rizi R Optimal Transfer of Spin-Order between a Singlet Nuclear Pair and a Heteronucleus. J. Magn. Reson 2010, 205, 9–13. [PubMed: 20427216]
32. Cai C; Coffey AM; Shchepin RV; Chekmenev EY; Waddell KW Efficient Transformation of Parahydrogen Spin Order into Heteronuclear Magnetization. J. Phys. Chem. B 2013, 117, 1219–1224. [PubMed: 23214962]
33. Haake M; Natterer J; Bargon J Efficient NMR Pulse Sequences to Transfer the Parahydrogen-Induced Polarization to Hetero Nuclei. J. Am. Chem. Soc 1996, 118, 8688–8691.
34. Hövener J-B; Chekmenev EY; Harris KC; Perman W; Tran T; Ross BD; Bhattacharya P Quality Assurance of Pasadena Hyperpolarization for 13C Biomolecules. Magn. Reson. Mater. Phy 2009, 22, 123–134.
35. Bär S; Lange T; Leibfritz D; Hennig J; Elverfeldt D.v.; Hövener J-B On the Spin Order Transfer from Parahydrogen to Another Nucleus. J. Magn. Reson 2012, 225, 25–35. [PubMed: 23103392]
36. Waddell KW; Coffey AM; Chekmenev EY In Situ Detection of Phip at 48 mT: Demonstration Using a Centrally Controlled Polarizer. J. Am. Chem. Soc 2011, 133, 97–101. [PubMed: 21141960]

37. Coffey AM; Shchepin RV; Wilkens K; Waddell KW; Chekmenev EY A Large Volume Double Channel 1H-X RF Probe for Hyperpolarized Magnetic Resonance at 0.0475 Tesla. J. Magn. Reson 2012, 220, 94–101. [PubMed: 22706029]
38. Stevanato G Alternating Delays Achieve Polarization Transfer (ADAPT) to Heteronuclei in PHIP Experiments. J. Magn. Reson 2017, 274, 148–162. [PubMed: 27894879]
39. Pravdivtsev AN; Yurkovskaya AV; Lukzen NN; Ivanov KL; Vieth H-M Highly Efficient Polarization of Spin-1/2 Insensitive NMR Nuclei by Adiabatic Passage through Level Anticrossings. J. Phys. Chem. Lett 2014, 5, 3421–3426. [PubMed: 26278456]
40. Reineri F; Viale A; Giovenzana G; Santelia D; Dastru W; Gobetto R; Aime S New Hyperpolarized Contrast Agents for C-13-MRI from Para-Hydrogenation of Oligooxyethylenic Alkynes. J. Am. Chem. Soc 2008, 130, 15047–15053. [PubMed: 18922000]
41. Shchepin RV; Barskiy DA; Coffey AM; Manzanera Esteve IV; Chekmenev EY Efficient Synthesis of Molecular Precursors for Para-Hydrogen-Induced Polarization of Ethyl Acetate-1–13C and Beyond. Angew. Chem. Int. Ed 2016, 55, 6071–6074.
42. Reineri F; Boi T; Aime S Parahydrogen Induced Polarization of 13C Carboxylate Resonance in Acetate and Pyruvate. Nat. Commun 2015, 6, 5858. [PubMed: 25556844]
43. Coffey AM; Shchepin RV; Feng B; Colon RD; Wilkens K; Waddell KW; Chekmenev EY A Pulse Programmable Parahydrogen Polarizer Using a Tunable Electromagnet and Dual Channel NMR Spectrometer. J. Magn. Reson 2017, 284, 115–124. [PubMed: 29028543]
44. Agraz J; Grunfeld A; Li D; Cunningham K; Willey C; Pozos R; Wagner S Labview-Based Control Software for Para-Hydrogen Induced Polarization Instrumentation. Rev. Sci. Instrum 2014, 85, 044705. [PubMed: 24784636]
45. Reineri F; Santelia D; Viale A; Cerutti E; Poggi L; Tichy T; Premkumar SSD; Gobetto R; Aime S Para-Hydrogenated Glucose Derivatives as Potential C-13-Hyperpolarized Probes for Magnetic Resonance Imaging. J. Am. Chem. Soc 2010, 132, 7186–7193. [PubMed: 20441193]
46. Reineri F; Viale A; Ellena S; Alberti D; Boi T; Giovenzana GB; Gobetto R; Premkumar SSD; Aime S N-15 Magnetic Resonance Hyperpolarization Via the Reaction of Parahydrogen with N-15-Propargylcholine. J. Am. Chem. Soc 2012, 134, 11146–11152. [PubMed: 22663300]
47. Cavallari E; Carrera C; Boi T; Aime S; Reineri F Effects of Magnetic Field Cycle on the Polarization Transfer from Parahydrogen to Heteronuclei through Long-Range J-Couplings. J. Phys. Chem. B 2015, 119, 10035–10041. [PubMed: 26161454]
48. Cavallari E; Carrera C; Aime S; Reineri F C-13 MR Hyperpolarization of Lactate by Using Parahydrogen and Metabolic Transformation in Vitro. Chem. Eur. J 2017, 23, 1200–1204. [PubMed: 27870463]
49. Chukanov NV; Salnikov OG; Shchepin RV; Kovtunov KV; Koptyug IV; Chekmenev EY Synthesis of Unsaturated Precursors for Parahydrogen-Induced Polarization and Molecular Imaging of 1–13C-Acetates and 1–13C-Pyruvates Via Side Arm Hydrogenation. ACS Omega 2018, 3, 6673–6682. [PubMed: 29978146]
50. Cavallari E; Carrera C; Aime S; Reineri F Studies to Enhance the Hyperpolarization Level in PHIP-SAH-Produced C13-Pyruvate. J. Magn. Reson 2018, 289, 12–17. [PubMed: 29448129]
51. Golman K; in't Zandt R; Thaning M Real-Time Metabolic Imaging. Proc. Natl. Acad. Sci. U. S. A 2006, 103, 11270–11275. [PubMed: 16837573]
52. Albers MJ; Bok R; Chen AP; Cunningham CH; Zierhut ML; Zhang VY; Kohler SJ; Tropp J; Hurd RE; Yen Y-F, et al. Hyperpolarized C-13 Lactate, Pyruvate, and Alanine: Noninvasive Biomarkers for Prostate Cancer Detection and Grading. Cancer Res 2008, 68, 8607–8615. [PubMed: 18922937]
53. Day SE; Kettunen MI; Gallagher FA; Hu DE; Lerche M; Wolber J; Golman K; Ardenkjaer-Larsen JH; Brindle KM Detecting Tumor Response to Treatment Using Hyperpolarized C-13 Magnetic Resonance Imaging and Spectroscopy. Nat. Med 2007, 13, 1382–1387. [PubMed: 17965722]
54. Yen YF; Kohler SJ; Chen AP; Tropp J; Bok R; Wolber J; Albers MJ; Gram KA; Zierhut ML; Park I, et al. Imaging Considerations for in Vivo C-13 Metabolic Mapping Using Hyperpolarized C-13-Pyruvate. Magn. Reson. Med 2009, 62, 1–10. [PubMed: 19319902]
55. Comment A; Merritt ME Hyperpolarized Magnetic Resonance as a Sensitive Detector of Metabolic Function. Biochemistry 2014, 53, 7333–7357. [PubMed: 25369537]

56. Merritt M; Harrison C; Storey C; Jeffrey F; Sherry A; Malloy C Hyperpolarized C-13 Allows a Direct Measure of Flux through a Single Enzyme-Catalyzed Step by NMR. Proc. Natl. Acad. Sci. U. S. A 2007, 104, 19773–19777. [PubMed: 18056642]
57. Hurd RE; Yen Y-F; Mayer D; Chen A; Wilson D; Kohler S; Bok R; Vigneron D; Kurhanewicz J; Tropp J, et al. Metabolic Imaging in the Anesthetized Rat Brain Using Hyperpolarized 1-C-13 Pyruvate and 1-C-13 Ethyl Pyruvate. Magn. Reson. Med 2010, 63, 1137–1143. [PubMed: 20432284]
58. Nelson SJ; Kurhanewicz J; Vigneron DB; Larson PEZ; Harzstark AL; Ferrone M; van Criekinge M; Chang JW; Bok R; Park I, et al. Metabolic Imaging of Patients with Prostate Cancer Using Hyperpolarized 1-C-13 Pyruvate. Sci. Transl. Med 2013, 5, 198ra108.
59. Lai M; Gruetter R; Lanz B Progress Towards In vivo Brain 13C-MRS in Mice: Metabolic Flux Analysis in Small Tissue Volumes. Anal. Biochem 2017, 529, 229–244. [PubMed: 28119064]
60. Morris P; Bachelard H Reflections on the Application of 13C-MRS to Research on Brain Metabolism. NMR Biomed 2003, 16, 303–312. [PubMed: 14679497]
61. Befroy DE; Perry RJ; Jain N; Dufour S; Cline GW; Trimmer J; Brosnan J; Rothman DL; Petersen KF; Shulman GI Direct Assessment of Hepatic Mitochondrial Oxidative and Anaplerotic Fluxes in Humans Using Dynamic 13C Magnetic Resonance Spectroscopy. Nat. Med 2014, 20, 98–102. [PubMed: 24317120]
62. Petersen KF; Befroy DE; Dufour S; Rothman DL; Shulman GI Direct Assessment of Hepatic Mitochondrial Oxidation and Pyruvate Cycling in Non Alcoholic Fatty Liver Disease by 13C Magnetic Resonance Spectroscopy. Cell Metab 2016, 24, 167–171. [PubMed: 27411016]
63. Mishkovsky M; Comment A; Gruetter R In Vivo Detection of Brain Krebs Cycle Intermediate by Hyperpolarized Magnetic Resonance. J. Cereb. Blood Flow Metab 2012, 32, 2108–2113. [PubMed: 22990416]
64. Jensen PR; Peitersen T; Karlsson M; in't Zandt R; Gisselsson A; Hansson G; Meier S; Lerche MH Tissue-Specific Short Chain Fatty Acid Metabolism and Slow Metabolic Recovery after Ischemia from Hyperpolarized NMR in Vivo. J. Biol. Chem 2009, 284, 36077–36082. [PubMed: 19861411]
65. Cavallari E; Carrera C; Sorge M; Bonne G; Muchir A; Aime S; Reineri F The 13c Hyperpolarized Pyruvate Generated by Parahydrogen Detects the Response of the Heart to Altered Metabolism in Real Time. Sci. Rep 2018, 8, 8366. [PubMed: 29849091]
66. Yoshihara HAI; Can E; Karlsson M; Lerche MH; Schwitter J; Comment A High-Field Dissolution Dynamic Nuclear Polarization of [1–13C]Pyruvic Acid. Phys. Chem. Chem. Phys 2016, 18, 12409–12413. [PubMed: 27093499]
67. Korchak S; Mamone S; Glöggler S Over 50 % 1H and 13C Polarization for Generating Hyperpolarized Metabolites—a Para-Hydrogen Approach. ChemistryOpen 2018, 7, 672–676. [PubMed: 30191091]
68. Shchepin RV; Pham W; Chekmenev EY Dephosphorylation and Biodistribution of 1–13C-Phospholactate in Vivo. J. Labelled Comp. Radiopharm 2014, 57, 517–524. [PubMed: 24995802]
69. Shchepin RV; Coffey AM; Waddell KW; Chekmenev EY Parahydrogen Induced Polarization of 1–13C-Phospholactate-D2 for Biomedical Imaging with >30,000,000-Fold NMR Signal Enhancement in Water. Anal. Chem 2014, 86, 5601–5605. [PubMed: 24738968]
70. Pravica MG; Weitekamp DP Net NMR Alighnment by Adiabatic Transport of Parahydrogen Addition Products to High Magnetic Field. Chem. Phys. Lett 1988, 145, 255–258.
71. Hirschbein BL; Mazenod FP; Whitesides GM Synthesis of Phosphoenolpyruvate and Its Use in Adenosine-Triphosphate Cofactor Regeneration. J. Org. Chem 1982, 47, 3765–3766.
72. Shchepin RV; Jaigirdar L; Chekmenev EY Spin-Lattice Relaxation of Hyperpolarized Metronidazole in Signal Amplification by Reversible Exchange in Micro-Tesla Fields. J. Phys. Chem. C 2018, 122, 4984–4996.
73. Ducker EB; Kuhn LT; Munnemann K; Griesinger C Similarity of SABRE Field Dependence in Chemically Different Substrates. J. Magn. Reson 2012, 214, 159–165. [PubMed: 22153915]
74. Norcott P; Burns MJ; Rayner PJ; Mewis RE; Duckett SB Using 2H Labelling to Improve the NMR Detectability of Pyridine and Its Derivatives by SABRE. Magn. Reson. Chem 2018, 56, 663–671. [PubMed: 29274294]

75. Taglang C; Korenchan DE; von Morze C; Yu J; Najac C; Wang S; Blecha JE; Subramaniam S; Bok R; VanBrocklin HF, et al. Late-Stage Deuteration of 13C-Enriched Substrates for T1 Prolongation in Hyperpolarized 13C MRI. Chem. Comm 2018, 54, 5233–5236. [PubMed: 29726563]

76. Aime S; Gobetto R; Reineri F; Canet D Hyperpolarization Transfer from Parahydrogen to Deuterium Via Carbon-13. J. Chem. Phys 2003, 119, 8890–8896.

77. Shchepin RV; Coffey AM; Waddell KW; Chekmenev EY Parahydrogen-Induced Polarization with a Rh-Based Monodentate Ligand in Water. J. Phys. Chem. Lett 2012, 3, 3281–3285. [PubMed: 23227297]

78. Schmidt AB; Berner S; Schimpf W; Müller C; Lickert T; Schwaderlapp N; Knecht S; Skinner JG; Dost A; Rovedo P, et al. Liquid-State Carbon-13 Hyperpolarization Generated in an MRI System for Fast Imaging. Nat. Commun 2017, 8, 14535. [PubMed: 28262691]

79. McClure R; Ong H; Janve V; Barton S; Zhu M; Li B; Dawes M; Jerome WG; Anderson A; Massion P, et al. Aerosol Delivery of Curcumin Reduced Amyloid-Beta Deposition and Improved Cognitive Performance in a Transgenic Model of Alzheimer's Disease. J. Alzheimers Dis 2017, 55, 797–811. [PubMed: 27802223]

80. Larson PEZ; Hu S; Lustig M; Kerr AB; Nelson SJ; Kurhanewicz J; Pauly JM; Vigneron DB Fast Dynamic 3D MR Spectroscopic Imaging with Compressed Sensing and Multiband Excitation Pulses for Hyperpolarized 13C Studies. Magn. Reson. Med 2011, 65, 610–619. [PubMed: 20939089]

81. von Morze C; Sukumar S; Reed GD; Larson PEZ; Bok RA; Kurhanewicz J; Vigneron DB Frequency-Specific SSFP for Hyperpolarized C-13 Metabolic Imaging at 14.1 T. Magn. Reson. Imaging 2013, 31, 163–170. [PubMed: 22898680]

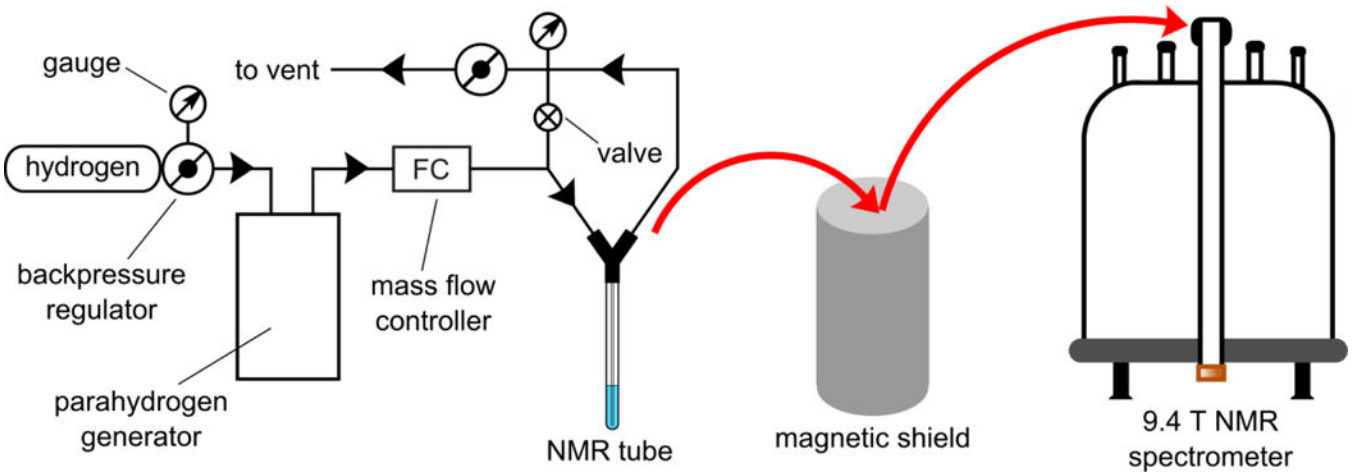

Figure 1.

Diagram of experimental setup for ^{13}C hyperpolarization and NMR spectroscopic detection of 1-^{13}C-phospholactate (PLAC) or 1-^{13}C-phospholactate-d_2 (PLAC-d_2). The safety valve indicated as ⊘ was set to 70 psig. Adopted with permission from ref. [49], Copyright (2018) American Chemical Society https://pubs.acs.org/doi/abs/10.1021%2Facsomega.8b00983

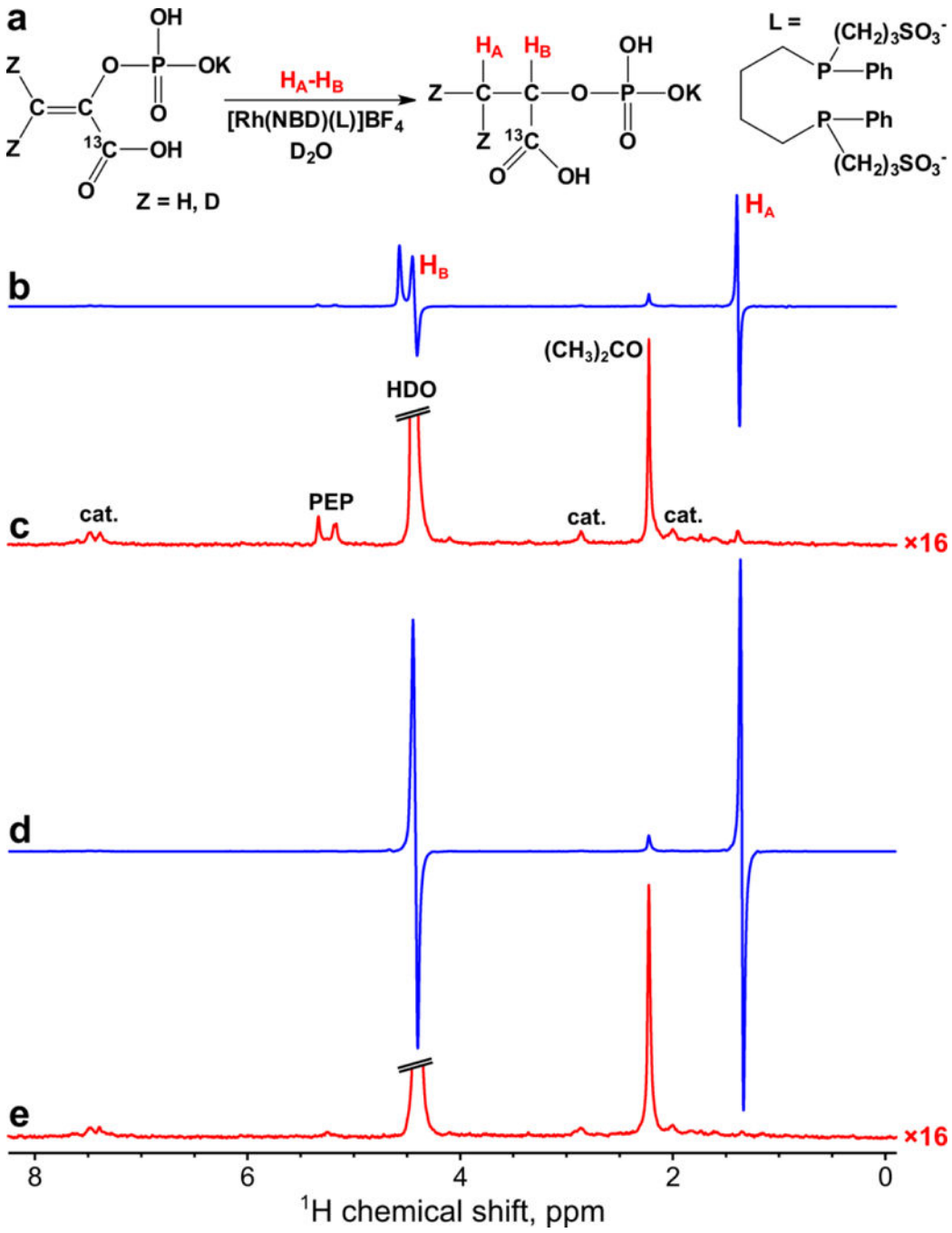

Figure 2.

(a) Scheme of phosphoenolpyruvate hydrogenation with p-H_2 producing HP 1-^{13}C-phospholactate with optional deuterium labeling (denoted as Z = H or D). (b-c) ^{1}H NMR spectra acquired in PASADENA hyperpolarization of non-deuterated 1-^{13}C-phospholactate (b) immediately after termination of p-H_2 bubbling and (c) after relaxation of hyperpolarization. (d-e) ^{1}H NMR spectra acquired in PASADENA hyperpolarization of 1-^{13}C-phospholactate-d_2 (d) immediately termination of p-H_2 bubbling and (e) after relaxation of hyperpolarization. Note that spectra (c) and (e) are multiplied by a factor of 16.

p-H_2 was bubbled for ~5 s at 140 sccm flow rate and 70 psig total pressure. H_A and H_B are the two spin-correlated p-H_2 derived protons.

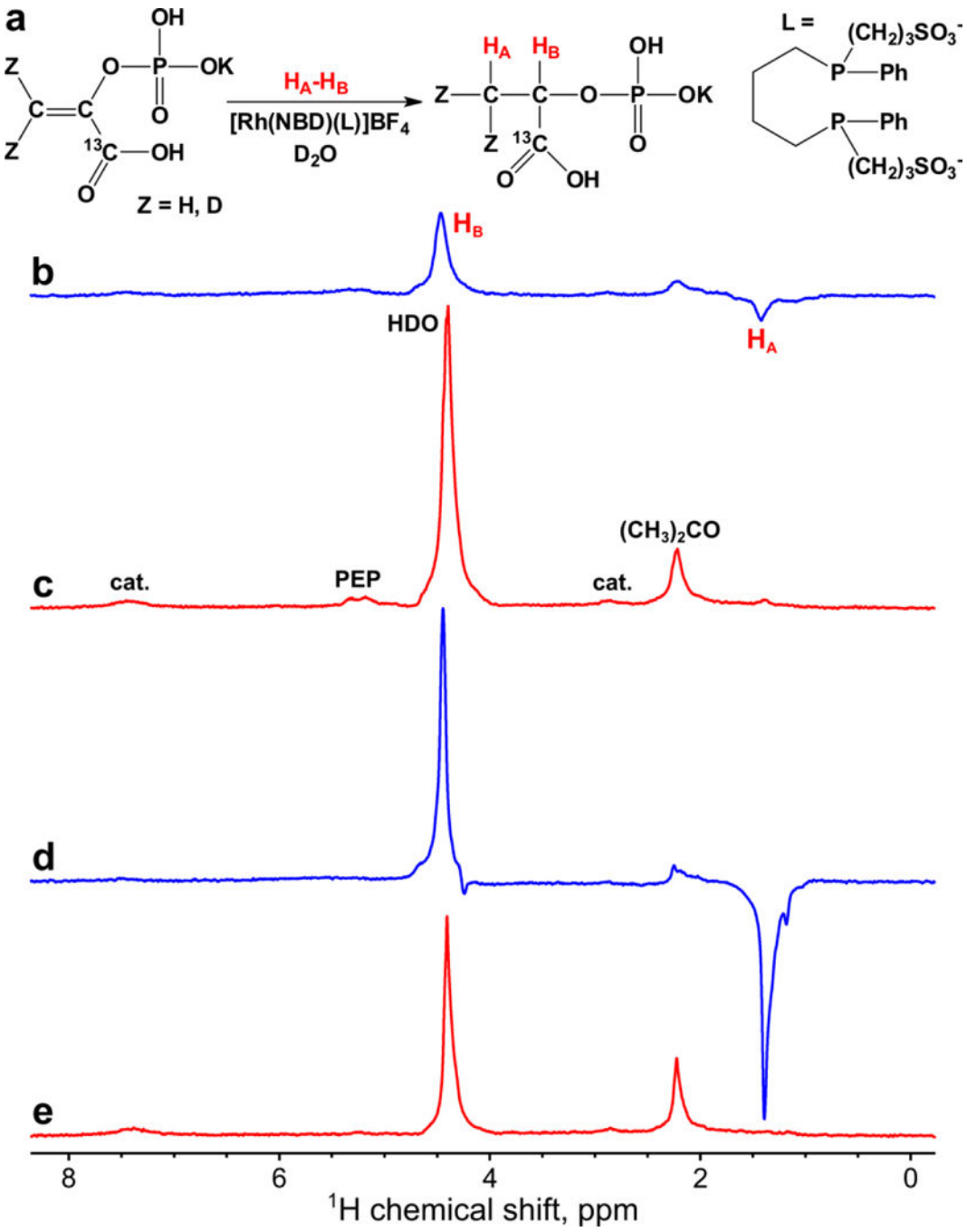

Figure 3.

(a) Scheme of phosphoenolpyruvate hydrogenation with p-H_2 producing HP 1-^{13}C-phospholactate with optional deuterium labeling (denoted as Z = H or D). (b-c) ^{1}H NMR spectra acquired in ALTADENA hyperpolarization of non-deuterated 1-^{13}C-phospholactate (b) immediately after the placement of the sample inside the NMR probe and (c) after relaxation of hyperpolarization. (d-e) ^{1}H NMR spectra acquired in ALTADENA hyperpolarization of 1-^{13}C-phospholactate-d_2 (d) immediately after the placement of the sample inside the NMR probe and (e) after relaxation of hyperpolarization. p-H_2 was

bubbled for ~5 s at 140 sccm flow rate and 70 psig total pressure. H_A and H_B are the two spin-correlated p-H_2 derived protons.

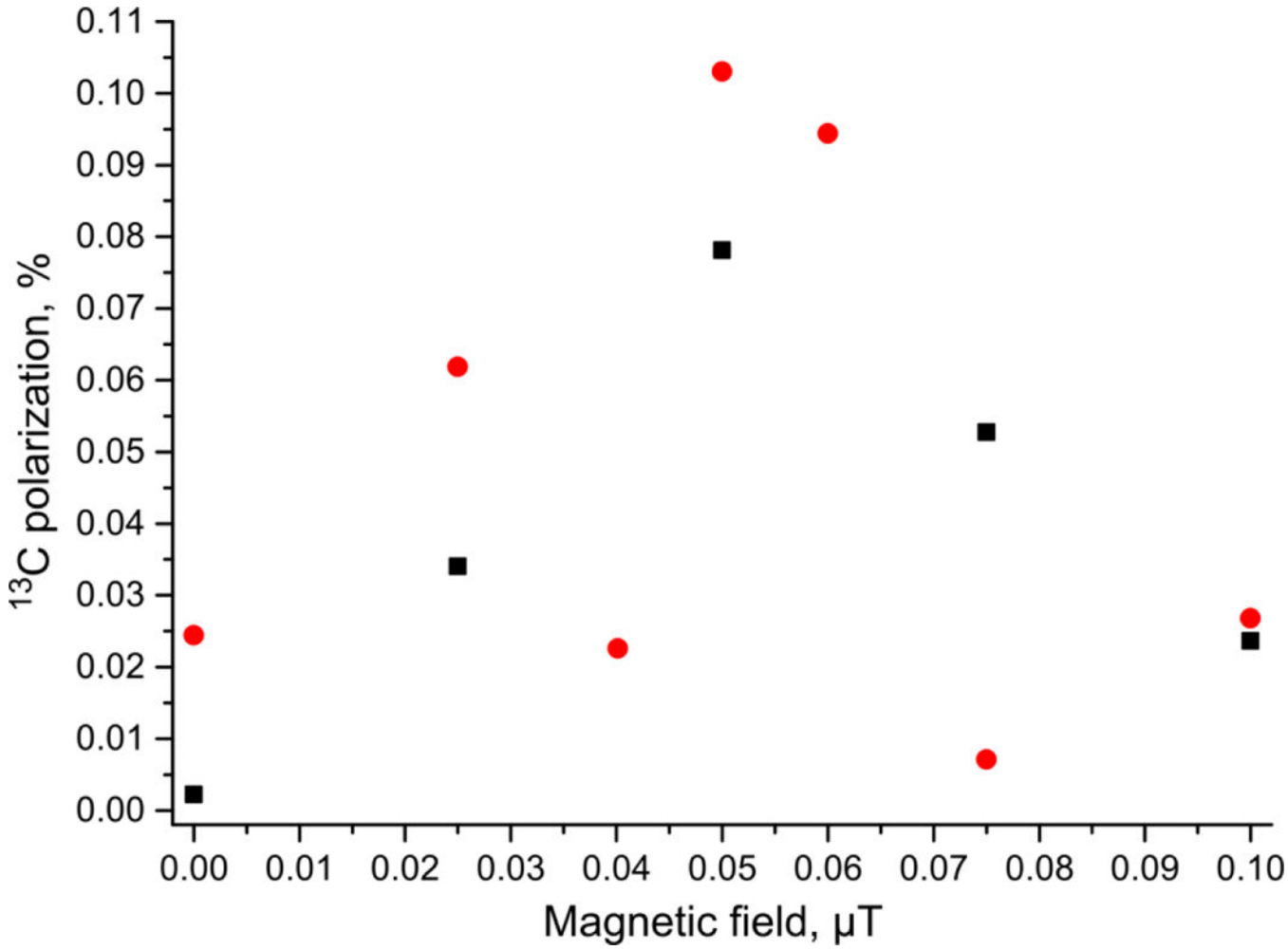

Figure 4.

Dependence of ^{13}C polarization of 1-^{13}C-phospholactate (black squares) and 1-^{13}C-phospholactate-d_2 (red circles) on magnetic field (produced by the solenoid) employed in MFC experiments. ^{13}C polarizations correspond to 85% p-H_2 fraction. Duration of p-H_2 bubbling was ~5 s. Note the mu-metal shield provides an isolation by approximately 1,200-fold according to the manufacturer's specifications; therefore, the use of the shield in the Earth's magnetic field results in the minimum residual magnetic field of approximately 40 nT, which corresponds to the zero mark on x-axis. The addition of the magnetic field (which was carefully calibrated by the gaussmeter and then attenuated by the resistor banks[72]) via the solenoid (see Methods for details) adds or subtracts the magnetic field from the residual value (40 nT)—therefore, the maximum observed at 40–50 nT in this plot is not surprising, because it likely corresponds to the null point, where the residual field is compensated by the induced field of the solenoid.

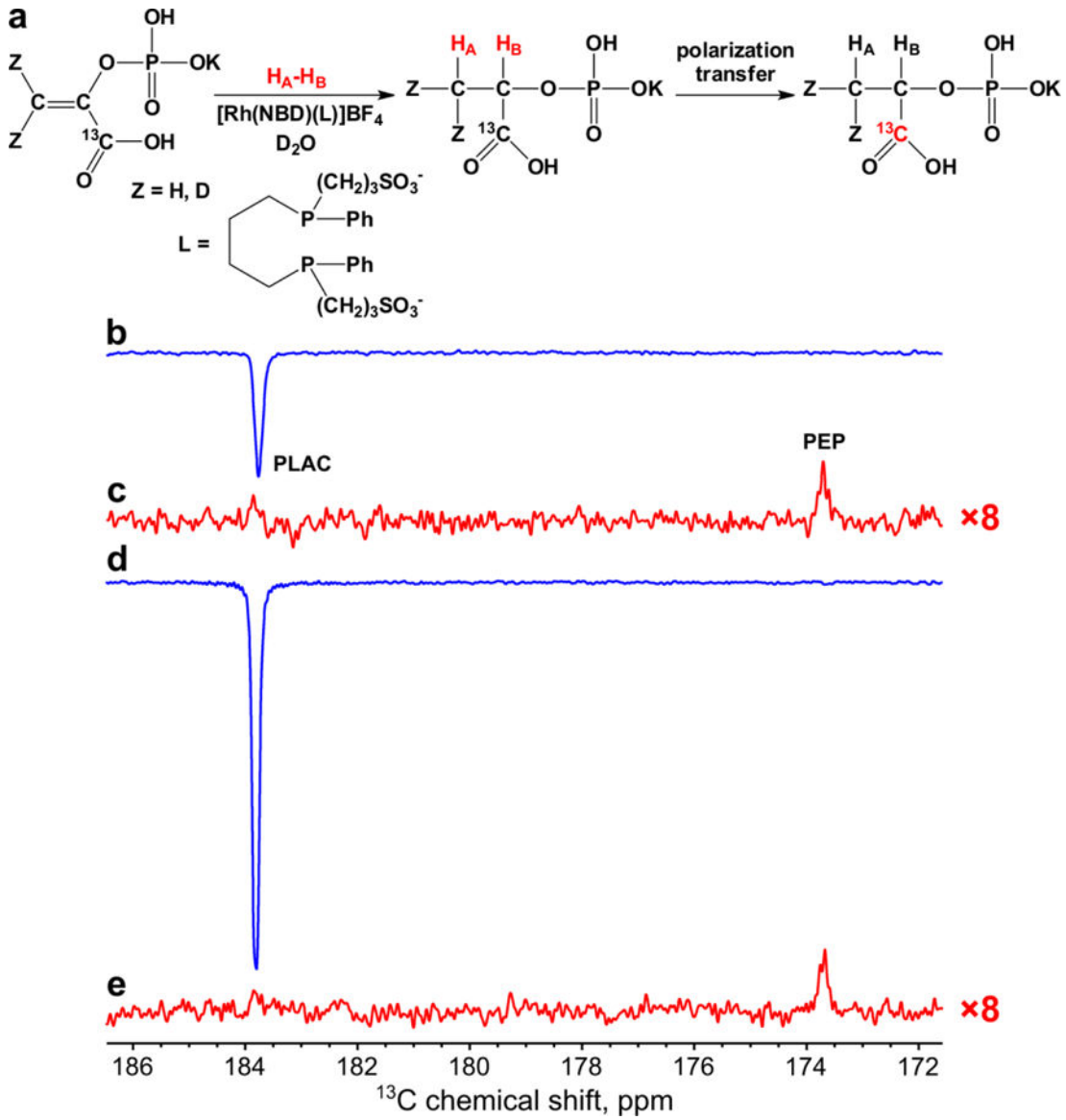

Figure 5.

(a) Scheme of 1-^{13}C-phosphoenolpyruvate hydrogenation with p-H_2 and polarization transfer via MFC producing ^{13}C HP phospholactate with optional deuterium labeling (denoted as Z = H or D). (b-c) ^{1}H NMR spectra acquired in MFC experiments for ^{13}C hyperpolarization of non-deuterated 1-^{13}C-phospholactate (b) immediately after termination of p-H_2 bubbling and (c) after relaxation of hyperpolarization. (d-e) ^{1}H NMR spectra acquired in MFC experiments for ^{13}C hyperpolarization of 1-^{13}C-phospholactate-d_2 (d) immediately termination of p-H_2 bubbling and (e) after relaxation of hyperpolarization. Note that spectra (c) and (e) are multiplied by a factor of 8. p-H_2 was bubbled for ~5 s at 140 sccm flow rate and 70 psig total pressure. H_A and H_B are the two spin-correlated p-H_2 derived protons.

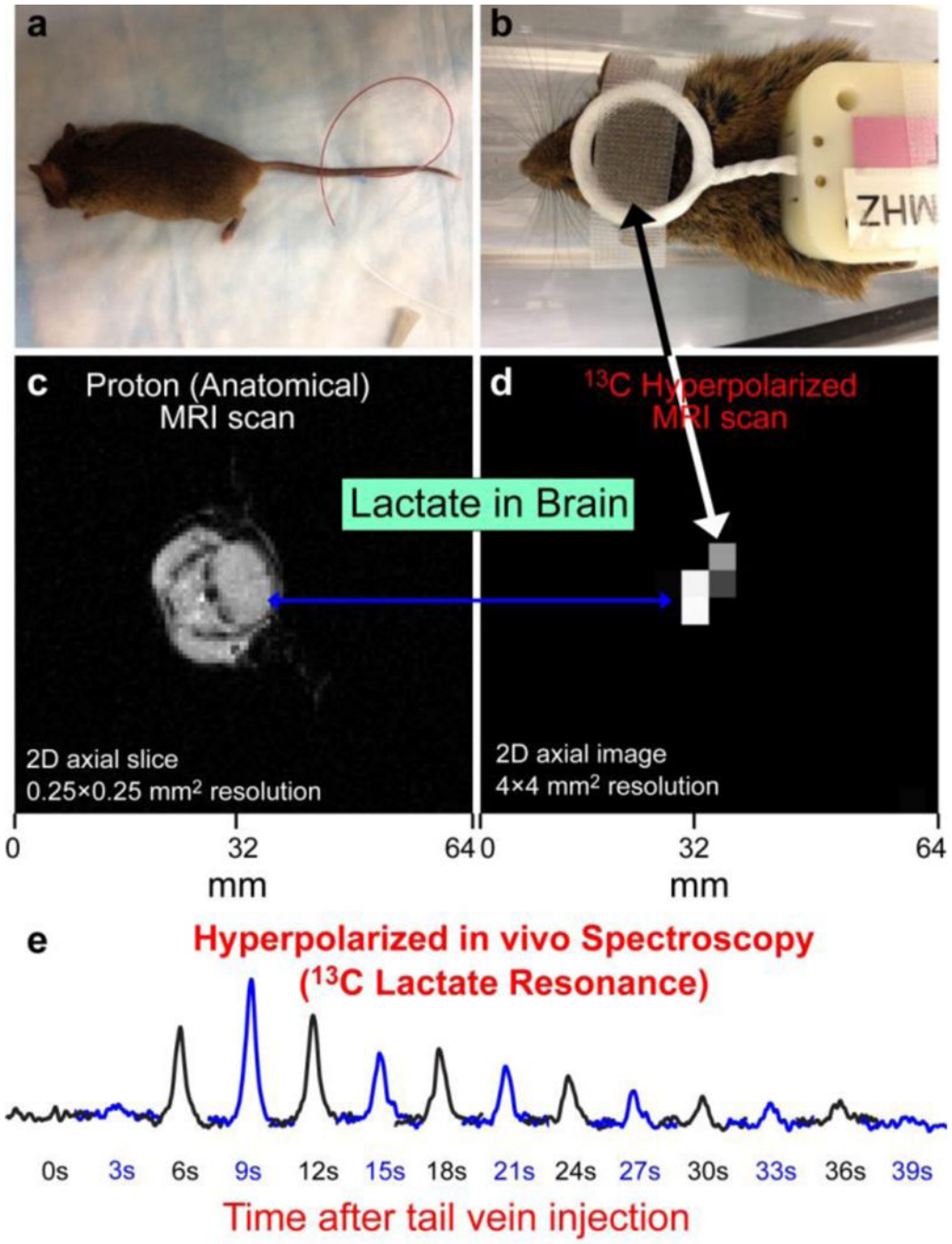

Figure 6.

(a) The photograph of an anesthetized animal with tail vein catheter installed. (b) The photograph of the same animal with the ^{13}C surface RF coil placed over the animal head. (c) 2D proton anatomical MRI image with slice selection via RF pulse sequences. (d) 2D ^{13}C projection MRI obtained after injection of HP PLAC-d_2; the RF-pulse sequence slice selection was not employed to maximize signal-to-noise ratio (SNR). (e) Non-localized ^{13}C NMR spectroscopy recorded immediately after tail-vein injection of the HP PLAC-d_2. ^{13}C region selectivity over the brain in displays (d) and (e) was achieved through the use of the

surface RF coil (shown in display (b)), which has detection primarily over the brain region. All images and spectra are recorded using Varian 4.7 T small-animal MRI scanner.

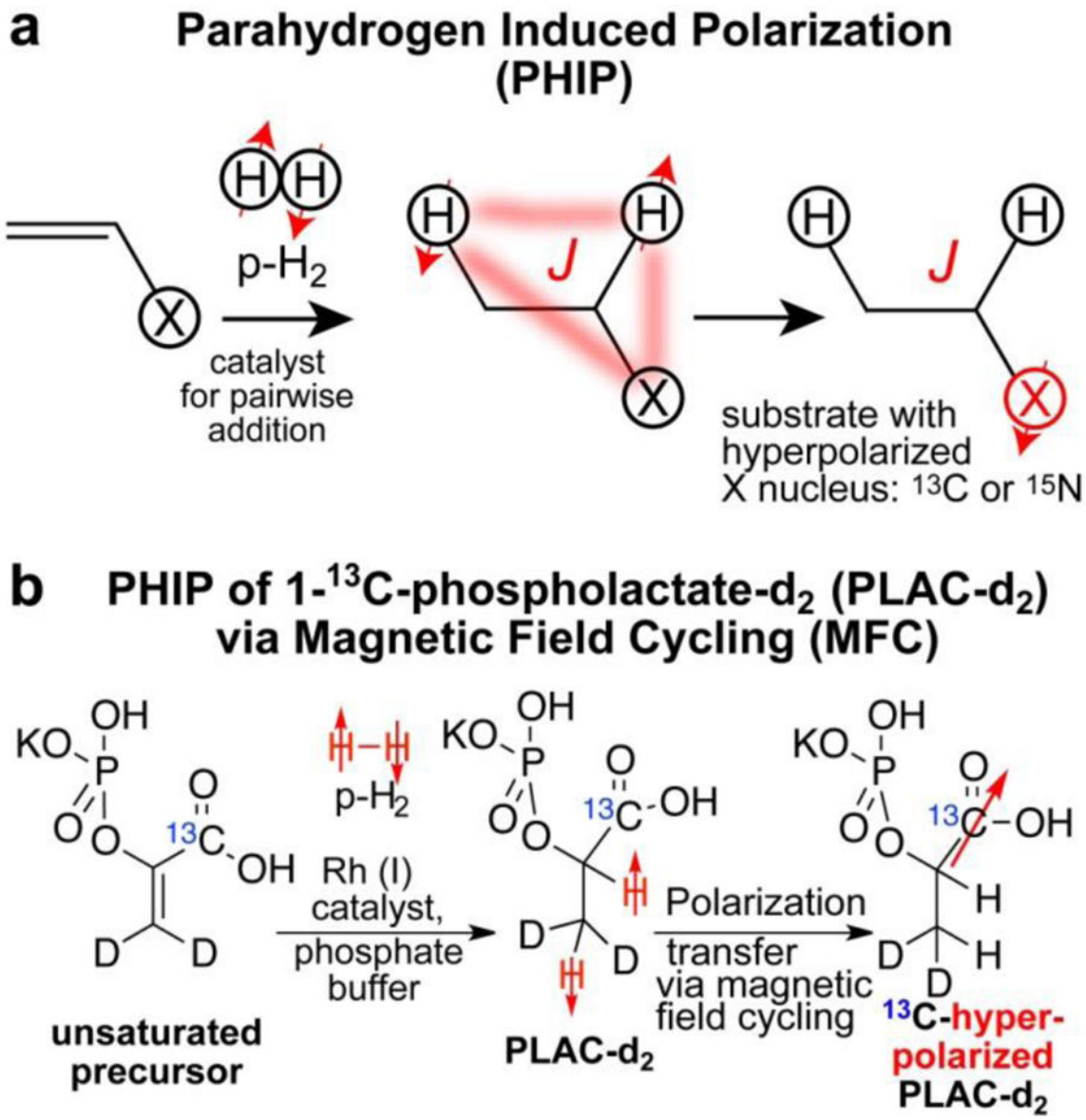

Scheme 1.

a) Schematic of Parahydrogen Induced Polarization (PHIP) Process with polarization transfer to heteronuclei.[5] (b) Schematic of PHIP hyperpolarization of 1-^{13}C-phospholactate-d_2 (PLAC-d_2) by pairwise p-H_2 addition to unsaturated precursor (1-^{13}C-phosphoenolpyruvate-d_2). Magnetic field cycling (MFC) procedure is employed in the second step for polarization transfer from p-H_2-derived protons to ^{13}C nucleus.

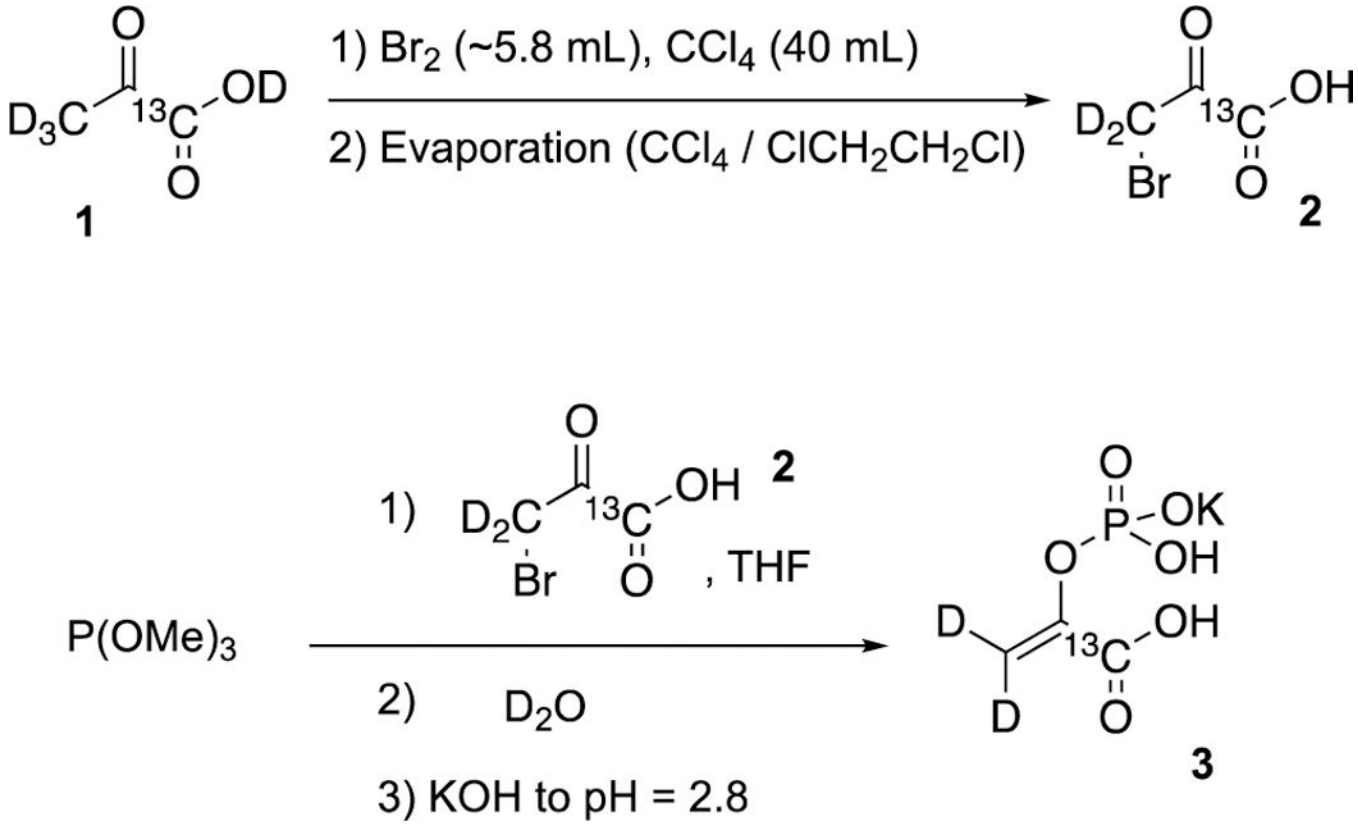

Scheme 2.
Synthesis of 1-^{13}C-phosphoenolpyruvate-d_2 (PEP-d_2).

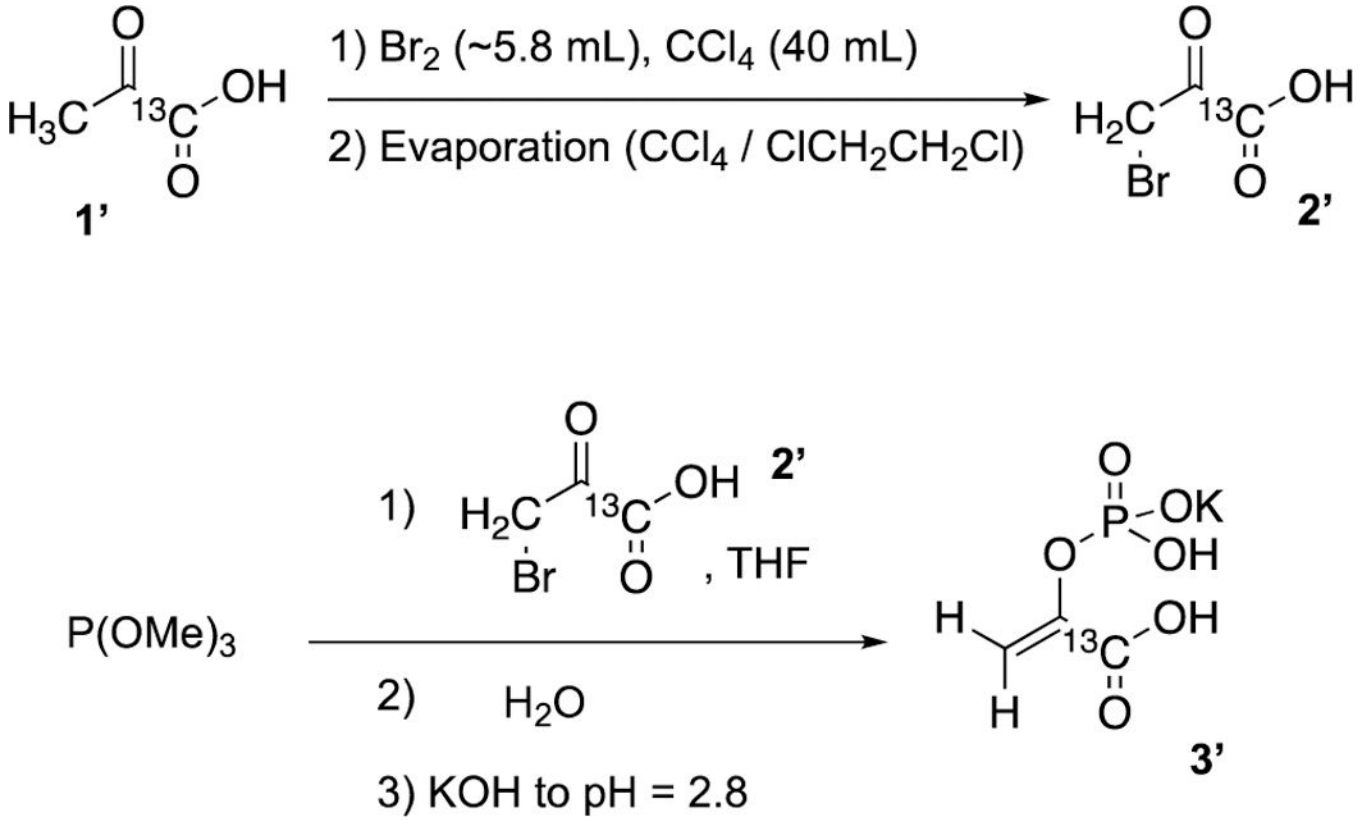

Scheme 3.
Synthesis of 1-^{13}C-phosphoenolpyruvate (PEP).